Why Do Model Tropical Cyclones Intensify More Rapidly at Low Latitudes?

ROGER K. SMITH AND GERARD KILROY

Meteorological Institute, Ludwig-Maximilians University of Munich, Munich, Germany

MICHAEL T. MONTGOMERY

Department of Meteorology, Naval Postgraduate School, Monterey, California

(Manuscript received 11 March 2014, in final form 28 July 2014)

ABSTRACT

The authors examine the problem of why model tropical cyclones intensify more rapidly at low latitudes. The answer to this question touches on practically all facets of the dynamics and thermodynamics of tropical cyclones. The answer invokes the conventional spin-up mechanism, as articulated in classical and recent work, together with a boundary layer feedback mechanism linking the strength of the boundary layer inflow to that of the diabatic forcing of the meridional overturning circulation.

The specific role of the frictional boundary layer in regulating the dependence of the intensification rate on latitude is discussed. It is shown that, even if the tangential wind profile at the top of the boundary layer is held fixed, a simple, steady boundary layer model produces stronger low-level inflow and stronger, more confined ascent out of the boundary layer as the latitude is decreased, similar to the behavior found in a time-dependent, three-dimensional numerical model. In an azimuthally averaged view of the problem, the most prominent quantitative differences between the time-dependent simulations at 10° and 30°N are the stronger boundary layer inflow and the stronger ascent of air exiting the boundary layer, together with the much larger diabatic heating rate and its radial gradient above the boundary layer at the lower latitude. These differences, in conjunction with the convectively induced convergence of absolute angular momentum, greatly surpass the effects of rotational stiffness (inertial stability) and evaporative-wind feedback that have been proposed in some prior explanations.

1. Introduction

Several previous studies have reported idealized numerical model simulations of tropical cyclone intensification in a quiescent environment and have examined, inter alia, the effect of latitude on vortex evolution (e.g., DeMaria and Pickle 1988; Smith et al. 2011; Rappin et al. 2011; Li et al. 2012). In these studies, and in a recent study of our own reported herein, the model cyclones are found to intensify more rapidly and reach a higher mature intensity as the latitude in the model is reduced. These findings have important practical implications and call for a theoretical explanation. All the foregoing simulations focused on the prototype problem for tropical cyclone intensification, which considers the evolution of a prescribed, initially cloud-free axisymmetric vortex in a quiescent environment on an f plane as articulated in Van Sang et al. (2008). A review of DeMaria and Pickle (1988) and Rappin et al. (2011) is deferred until section 6, which offers also an appraisal of the explanations given in these papers and in Li et al. (2012).

There are two prominent theoretical studies that predict a different behavior to all of the references cited above. Carrier (1971) presented a theory of hurricane intensification in which the time scale of spinup is given by $2/f$, where f is the Coriolis parameter. This time scale is about 16 h for latitudes of interest considered by Carrier, and it emerges by determining the time required to flush the core of ambient tropical air and replace it with air characterized by a moist adiabatic state (F. Fendell 2011, personal communication). There are many ad hoc assumptions in the Carrier theory that, collectively, are difficult to assess in regard to the overall dynamics. Nevertheless, the spin-up rate from the

Corresponding author address: Prof. Roger K. Smith, Meteorological Institute, Ludwig-Maximilians University of Munich, Theresienstr. 37, 80333 Munich, Germany.
E-mail: roger.smith@lmu.de

DOI: 10.1175/JAS-D-14-0044.1

Carrier theory, which predicts that lower-latitude storms will spin up more slowly than higher-latitude storms, can be tested.

Many years after the Carrier theory was proposed, Emanuel (2003) summarized his intensification theory (see his section 3.2), wherein the time scale for intensification scales as $H/(C_D \mathrm{Vg}_{\max})$, where H is an atmospheric scale height ($\approx$8 km), C_D is the surface drag coefficient, and $\mathrm{Vg}_{\max}$ is the maximum gradient wind determined from the so-called potential intensity theory (Emanuel 1995; Bister and Emanuel 1998). For typical conditions, this time scale is on the order of 15 h. Emanuel (2003) did not reference Carrier (1971), but the typical time scale for development in the Emanuel theory is numerically close to that of Carrier's theory, yet it is independent of f at leading order. Emanuel's time-dependent theory for tropical cyclone intensification has undergone a reincarnation in recent years (Emanuel 2012). However, for reasons explained in Persing et al. (2013), Emanuel's formulations fall short of providing an acceptable theory for tropical cyclone intensification in three dimensions, which is the proper benchmark for comparison with reality. It will be demonstrated in this paper that neither the Carrier nor Emanuel theories correctly capture the proper dependence of intensification on the Coriolis parameter.

Smith et al. (2011) investigated the rotational constraint on the intensity and size of tropical cyclones using a minimal, three-layer, axisymmetric tropical cyclone model, similar to that of DeMaria and Pickle (1988), but formulated in σ coordinates and with a different representation of deep convection. In the first of two sets of experiments, the same baroclinic vortex was used to initialize the model and to examine the spin-up process in a quiescent environment with different levels of background rotation, characterized by a constant value of f. It was found that the rate of intensification, after some short gestation period (on the order of 15 h), increased monotonically with decreasing latitude of the cyclone environment, but that the strongest vortices, as characterized by their quasi-steady intensity after 12 days, develop in environments with intermediate background rotation. The main focus of Smith et al. (2011) was directed at understanding the control of ambient rotation on mature intensity and size and not on the spin-up phase. The reason for the greater spin-up rate at lower latitudes was not investigated. The result in regard to the mature intensity appeared to be in line with those of classical laboratory experiments by Turner and Lilly (1963), but the analogy was found to have certain limitations, including the fact that the spinup of the maximum tangential winds in the inner core of the model takes place in the boundary layer.

The results of Smith et al. (2011) were based on a simple axisymmetric model, and a question is whether similar results are found in three-dimensional, multilevel models. We have just completed such a study using the fifth-generation Pennsylvania State University–National Center for Atmospheric Research Mesoscale Model (MM5). While the results of this study have not yet been submitted for publication, a summary of the findings pertinent to the present paper is given in section 2. Similar idealized experiments to those described above have been reported in the recent literature by Rappin et al. (2011) and Li et al. (2012).

Li et al. (2012) carried out simulations at eight different latitudes (5°, 7.5°, 10°, 12.5°, 15°, 20°, 25°, and 30°N) and found also that vortex intensification at low latitudes is faster than at high latitudes. They attributed this result to the extent to which gradient wind balance is broken in the boundary layer. As explained in section 6, we have questions about their purported explanations, but their invocation of the role of boundary layer dynamics is, in part, consistent with a new paradigm for tropical cyclone intensification that has been expounded in a series of recent papers (Van Sang et al. 2008; Montgomery et al. 2009; Smith et al. 2009; Bui et al. 2009) and summarized by Montgomery and Smith (2014). In fact, as explained later, we think that the new paradigm provides a useful framework for explaining the dependence of the intensification rate on latitude.

The new intensification paradigm recognizes the presence of localized, rotating deep convection that grows in the cyclonic rotation–rich environment of the incipient storm. The updrafts within these convective structures greatly amplify the vorticity by vortex tube stretching. In an azimuthally averaged view of the new paradigm, the spinup of the maximum tangential winds takes place within the frictional boundary layer, although the spinup of the winds above the boundary layer (which are widely held to be in approximate gradient wind balance) is necessary as well.

As in the earlier paradigms, the spinup of the bulk vortex above the boundary layer occurs through the conventional mechanism articulated by Ooyama (1969, 1982) and others. In essence, deep convection is invoked as the mechanism that brings about the radial convergence of rings of air above the frictional boundary layer. These rings conserve their absolute angular momentum M, and as their radius deceases, they spin faster (sometimes known as "the ice skater effect"). In contrast to the conventional mechanism, the boundary layer spin-up mechanism is possible, because the inward displacement of air parcels is much larger in the boundary layer than above it, a consequence of the frictional disruption of gradient wind balance in that layer. This disruption leads

to a net inward force in the boundary layer. Since the azimuthal-mean tangential wind speed $v = M/r - (1/2)fr$, the possibility arises that the material loss of M to the surface may be more than offset by a large and rapid inward displacement of rings of air so that the tangential wind actually increases and eventually becomes larger than that above the boundary layer. In high-resolution model simulations, these processes are exemplified by the evolution of the azimuthally averaged M surfaces in time-height cross sections. These surfaces tilt inward with height within the boundary layer and outward with height above, with a ''nose'' at the top of the boundary layer. The evolution of the M surfaces during the intensification of a tropical cyclone has been documented observationally by Montgomery et al. (2014).

While the boundary layer spin-up mechanism presumes an increasing gradient wind and radial pressure gradient at the top of the boundary layer with time in association with the conventional mechanism, it contributes also to the spinup of the bulk vortex through the lofting of the enhanced tangential momentum into the bulk vortex and a corresponding adjustment of the wind and mass fields of the bulk vortex toward the higher winds from the boundary layer.

It is noteworthy that although Ooyama (1969) did not focus on the question of the latitudinal dependence of the spin-up rate, he did present a linearized version of his cooperative intensification model, in which the growth rate of a small-amplitude initial disturbance contains an explicit dependence on the Coriolis parameter [his Eq. (8.10)]. Inspection of the analytical growth rate that he derived reveals the same qualitative dependence of the intensification rate on latitude as in the other modeling studies discussed above. We will review the insights and predictions obtained from this formula in section 5. In light of the new spin-up paradigm discussed above, it is pertinent to note that Ooyama's (1969) model is axisymmetric and does not contain the boundary layer spin-up pathway.

In summary, on the system scale, the new spin-up paradigm has two dynamical components. The first is the conventional spin-up mechanism. The second component comprises the boundary layer spin-up mechanism summarized in the foregoing discussion. A related and essential ingredient of the new spin-up paradigm is the maintenance of convective instability in the inner-core region of the vortex by enhanced surface moisture fluxes, although the maintenance does not require the fluxes to continue to increase with wind speed (Montgomery et al. 2009, 2015).

The existence of the boundary layer spin-up mechanism is suggestive that boundary layer dynamics may be an important element of the explanation for the intensification rate of model tropical cyclones being a function of latitude. Estimating the relative role of the conventional mechanism and its dependence on latitude is an important objective of this study also. To test this idea here, we seek to isolate the effect of the boundary layer using simplified versions of the steady slab boundary layer model described in detail by Smith (2003), Smith and Vogl (2008), and Smith and Montgomery (2008). As it turns out, the explanation for the dependence of the intensification rate and mature intensity on latitude touches on practically all facets of the dynamics and thermodynamics of tropical cyclones.

The paper is organized as follows. First, in section 2 we outline the new results from our own calculations referred to earlier. Then, in section 3 we provide a summary of the simplified slab boundary layer model, and in section 4 we present a series of calculations from the boundary layer model. The implications of the results for our own and previous explanations for vortex behavior at different latitudes are discussed in sections 5 and 6, respectively. The conclusions are given in section 7.

2. The new calculations

The numerical experiments using MM5 referred to above are similar to those described in Van Sang et al. (2008). They are carried out using a modified version of the model (version 3.6.1). A detailed description of the model can be found in Grell et al. (1995). The model is configured with three domains: a coarse mesh of 45-km grid spacing and two, two-way nested domains of 15- and 5-km grid spacing. The domains are square and are 9000, 4500, and 1500 km on each side. Three calculations are performed on an f plane centered at latitudes 10°, 20°, and 30°N. The model has 24 σ levels in the vertical, 7 of which are below 850 hPa [see Smith and Thomsen (2010), section 2.1]. The vertical resolution in the boundary layer is believed to be adequate for correctly representing the boundary layer dynamics under the prescribed changes to the latitude of the vortex environment. For simplicity, there is no representation of dissipative heating.

Deep moist convection is represented explicitly using a warm-rain scheme, as in Montgomery et al. (2009). In addition, to retain simplicity, we choose the Blackadar boundary layer scheme, one of several available in the model. In this scheme, the surface drag and heat and moisture exchange coefficients are modified to fit the results of the Coupled Boundary Layer Air–Sea Transfer Experiment (CBLAST; Black et al. 2007). The surface exchange coefficients for sensible heat and moisture are set to the same constant, 1.2×10^{-3}. The drag coefficient is given by the following formula:

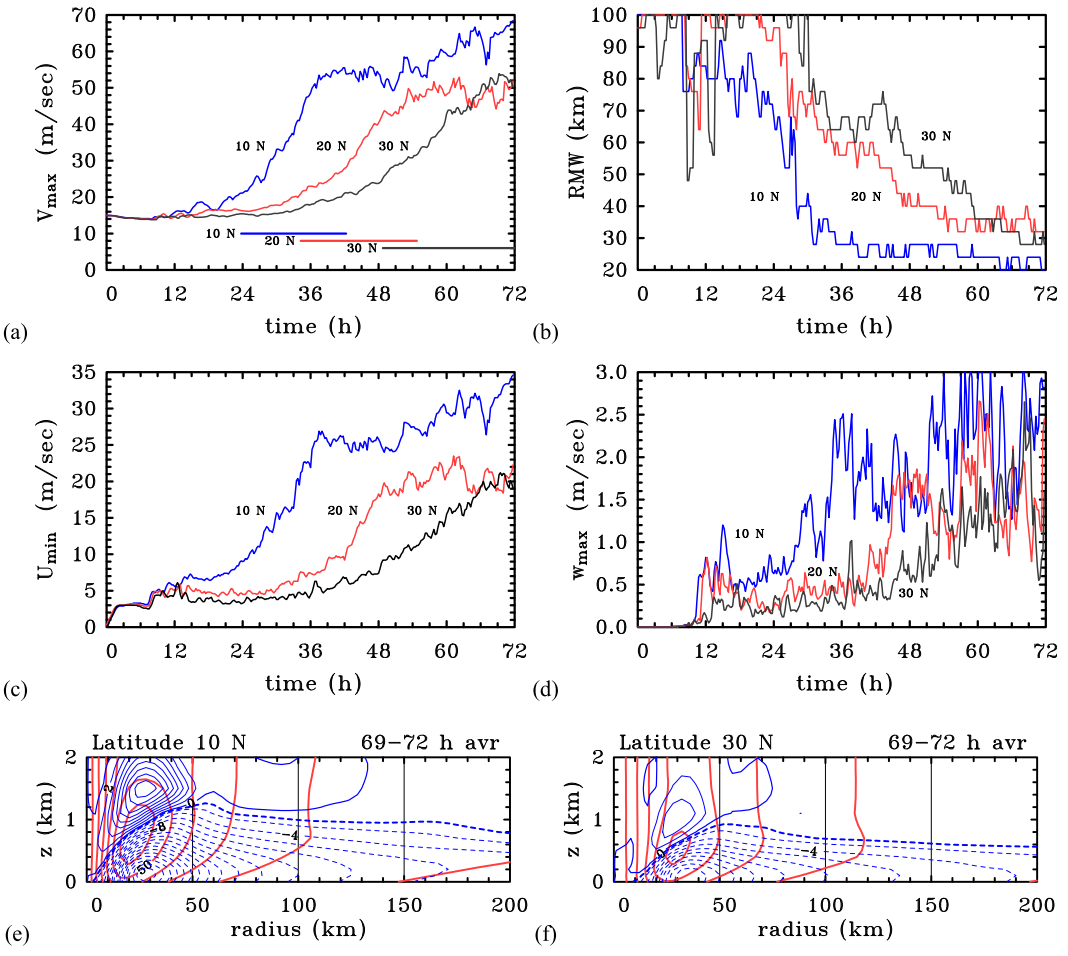

FIG. 1. Time series of azimuthally averaged quantities in calculations for the prototype intensification problem at latitudes 10°, 20°, and 30°N. (a) The maximum tangential wind speed; (b) the RMW; (c) the maximum radial inflow; and (d) the maximum vertical velocity. The horizontal lines in (a) show the period of rapid intensification (defined in the text) at each latitude and are referred to in Figs. 4 and 6. (e),(f) Vertical cross sections of the azimuthally averaged tangential (red contours) and radial wind (blue contours) in the lowest 2 km at 10° and 30°N, respectively (contour intervals: 10 m s^{-1} for the tangential wind and 2 m s^{-1} for the radial wind). Dashed curves indicate negative values; the thick dashed blue contour shows the -1 m s^{-1} contour of radial wind.

$$C_D = 0.7 \times 10^{-3} + 1.4 \times 10^{-3}[1 - \exp(-0.055|\mathbf{u}|)], \quad (1)$$

where $|\mathbf{u}|$ is the wind speed at the lowest model level. This formula is based on our interpretation of Fig. 5 from Black et al. (2007).

The warm-rain and boundary layer schemes are applied in all domains. No cumulus parameterization is used. The sea surface temperature is a constant (27°C). As the time period of the calculations is short (3 days), we have not implemented a radiative cooling scheme.

The initial vortex is axisymmetric, with a maximum tangential wind speed of 15 m s^{-1} at the surface at a radius of 100 km. The magnitude of the tangential wind decreases sinusoidally with height, vanishing at the top model level. The temperature field is initialized to be in gradient wind balance with the wind field using the method described by Smith (2006). The far-field temperature and humidity are based on the neutral sounding of Rotunno and Emanuel (1987).

Figures 1a–d show time series of azimuthally averaged quantities, including the maximum tangential wind speed V_{max} and the radius at which it occurs (RMW); the maximum radial inflow; and the maximum vertical velocity in the three calculations for different latitudes. Typically, at 10°N, the maximum tangential wind speed occurs at a height of 750 m, while at 30°N it is slightly lower, about 600 m. The maximum vertical velocity occurs at a height of between 10 and 14 km. As in the previous calculations referred to in the introduction, the rate of intensification increases with decreasing latitude so that, after a few days, the maximum

mature intensity is achieved at the lowest latitude (Fig. 1a). Consistent with the idea that the closer air parcels can approach the axis, the faster they can spin (see section 1), the RMW decreases also with latitude during the intensification phase (Fig. 1b). The larger inward displacement of air parcels is consistent with the increase in the maximum radial wind speeds as the latitude decreases. Finally, the maximum vertical velocity is largest for the vortex at 10°N, and this maximum decreases with increasing latitude (Fig. 1d). These results are broadly similar to those of Smith et al. (2011). Figures 1e and 1f show radius–height cross sections of the azimuthally averaged radial and tangential wind components averaged during the period from 69 to 72 h for the 10° and 30°N calculations. Noteworthy features relevant to the present study are the deeper boundary layer (as characterized, for example, by the depth of appreciable inflow indicated by the $-1\,\mathrm{m\,s^{-1}}$ radial velocity contour) at 10°N and the monotonic increase of boundary layer depth with decreasing radius to approximately the radius of maximum tangential wind speed, which, itself, occurs near the top of the appreciable inflow layer.

The longer-term behavior of the solutions will be discussed elsewhere. Suffice it to say, the vortices reach a maximum intensity after a week or more and eventually decay, as found also in the study by Smith et al. (2014) using a different model.

3. A simple boundary layer model

We review first the steady slab boundary layer model described by Smith and Vogl (2008), which provides a suitable framework to examine the issues raised above. A brief appraisal of the slab boundary layer is given in appendix A. For simplicity, we ignore here the thermodynamic processes that occur in the boundary layer and exclude the effects of mixing through the top of the inflow layer on account of shallow convection. Then, the remaining equations for the radial momentum, azimuthal momentum, and mass continuity can be written in the following forms:

$$u_b\frac{du_b}{dr}=\frac{w_{h-}}{h}u_b-\frac{(v_g^2-v_b^2)}{r}-f(v_g-v_b)-\frac{C_D}{h}(u_b^2+v_b^2)^{1/2}u_b, \tag{2}$$

$$u_b\frac{dv_b}{dr}=\frac{w_{h-}}{h}(v_b-v_g)-\left(\frac{v_b}{r}+f\right)u_b-\frac{C_D}{h}(u_b^2+v_b^2)^{1/2}v_b, \quad \text{and} \tag{3}$$

$$\frac{du_b}{dr}=-\frac{u_b}{r}-\frac{w_h}{h}, \tag{4}$$

where u_b and v_b are the vertically averaged radial and azimuthal components of wind speed in the boundary layer, $v_g(r)$ and w_h are the tangential wind speed and vertical velocity at the top of the boundary layer, f is the Coriolis parameter, C_D is the surface drag coefficient given by Eq. (1), and $w_{h-}=(1/2)(w_h-|w_h|)$. Consistent with the slab formulation, the quantities u_b and v_b are assumed to be independent of depth. Note that w_{h-} is nonzero only when $w_h<0$, in which case it is equal to w_h. Thus, the terms involving w_{h-} represent the transport of properties from above the boundary layer that may be different from those inside the boundary layer.

Substitution of Eq. (4) into Eq. (2) gives an expression for w_h:

$$w_h=\frac{h}{1+\alpha}\left\{\frac{1}{u_b}\left[\frac{v_g^2-v_b^2}{r}+f(v_g-v_b)+\frac{C_D}{h}(u_b^2+v_b^2)^{1/2}u_b\right]-\frac{u_b}{r}\right\}, \tag{5}$$

where α is zero if the expression in curly brackets is positive and unity if it is negative. With this expression for w_h, Eqs. (2), (3), and (5) form a system of ordinary differential equations that may be integrated radially inwards from some large radius R to determine u_b and v_b as functions of r, given values of these quantities at $r=R$ as well as the radial profile $v_g(r)$. We show examples of such solutions in section 4.

The foregoing equations are too complicated to afford simple insights about parameter dependencies, and it proves useful to examine a linear approximation thereto, even though, as shown by Smith and Montgomery (2008) and Vogl and Smith (2009), such an approximation cannot be justified in the inner-core region of a tropical cyclone.

Linear approximation

To examine possible approximations to the foregoing equations, it is convenient to take $v_b=v_g+v_b'$ and rewrite Eqs. (2) and (3) in the form

$$u_b\frac{du_b}{dr}=\frac{w_{h-}}{h}u_b+\frac{v_b'^2}{r}+\xi_g v_b'-\frac{C_D}{h}|\mathbf{v}_b|u_b \quad \text{and} \tag{6}$$

$$u_b\frac{dv_b'}{dr}=\frac{w_{h-}}{h}v_b'-\frac{u_b v_b'}{r}-\zeta_a u_b-\frac{C_D}{h}|\mathbf{v}_b|(v_g+v_b'), \tag{7}$$

where $\zeta_a=dv_g/dr+v_g/r+f$ is the absolute vorticity, and $\xi_g=2v_g/r+f$ is twice the absolute angular velocity of the gradient wind profile above the boundary layer. One approximation would be to linearize Eqs. (6) and (7) so that they become

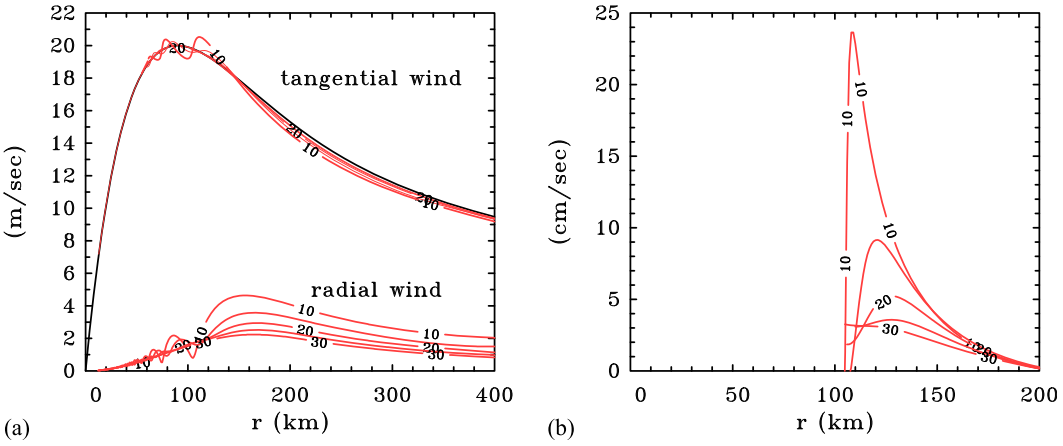

FIG. 2. (a) Radial profiles of radial and tangential wind components in the boundary layer for different values of latitude for a fixed profile of gradient wind at the top of the boundary layer (black line). (b) The corresponding profiles of vertical velocity at the top of the boundary layer [note the difference in the radial extent of the abscissa in (a) and (b)]. The calculations are based on the assumption of a fixed boundary layer depth of 1 km.

$$\xi_g v_b' = \frac{C_D v_g}{h} u_b \quad \text{and} \tag{8}$$

$$\zeta_a u_b = -\frac{C_D v_g^2}{h}. \tag{9}$$

These equations may be readily solved to yield

$$u_b = -\mu v_g \quad \text{and} \tag{10}$$

$$v_b' = -\sigma^2 v_g, \tag{11}$$

where $\mu = C_D v_g/(h\zeta_{ag})$, $\sigma = C_D v_g/(hI)$, and $I^2 = \xi_g \zeta_{ag}$ is the inertial stability of the flow above the boundary layer. Note that for finite values of μ and σ, $v_b' < 0$ so that the generation of supergradient winds ($v_b > v_g$) is precluded by the linear approximation. Clearly, the linear approximation requires that $|u_b|/v_g \ll 1$ and $|v_b'|/v_g \ll 1$; that is, $|\mu| \ll 1$ and $\sigma^2 \ll 1$. It applies to the limit of weak friction and is the slab equivalent of the classical Ekman boundary layer solution in which the net Coriolis force is balanced by the frictional force.

We are now in a position to examine the effect of changing latitude on the solution, the latitudinal dependence being implicit through the value of f in the expressions for μ and σ (or I). Equation (10) shows that an increase in latitude requires a smaller amount of inflow for the Coriolis force to balance the frictional force and Eq. (9) shows a similar result for the perturbation tangential wind. Thus, the local magnitudes of u_b and v_b' both decrease with increasing latitude. The results of these calculations, as well as numerical solutions of the full nonlinear system, are presented in the next section.

4. Boundary layer solutions for different latitudes

We show now solutions of Eqs. (2), (3), and (5) for a range of latitudes from 10° to 30°N, and for a constant-depth boundary layer. For comparison, we show also solutions of the linear approximation represented by Eqs. (10) and (11). In each case, the radial profile of gradient wind is given by the formula:

$$v_g = v_1 s \exp(-\alpha_1 s) + v_2 s \exp(-\alpha_2 s), \tag{12}$$

where v_1, v_2, α_1, and α_2 are constants with the values 25.9 m s^{-1}, 15 m s^{-1}, 1.0685, and 0.9, respectively, and $s = r/r_m$, r_m being the radius of maximum tangential wind speed.

a. Nonlinear constant-depth boundary layer

Figure 2 shows solutions for u_b, v_b, and w_b for a boundary layer with a constant depth of 1000 m and a gradient wind profile with a maximum tangential wind speed of 20 m s^{-1} at a radius of 90 km, corresponding with a weak tropical storm. It is seen that as the latitude decreases, the difference between the tangential wind and the gradient wind increases at all radii beyond about 140 km, whereas a little inside this radius, the tangential wind speed becomes supergradient ($v_b > v_g$) and the maximum tangential wind speed increases slightly with decreasing radius. At a fixed radius, the radial wind component increases also with decreasing latitude, the maximum inflow increasing from barely 3 m s^{-1} at 30°N to about 5 m s^{-1} at 10°N. Note also that the radius of maximum inflow decreases with decreasing latitude. When the tangential wind becomes supergradient, all forces in the radial momentum equation are directed radially outwards and the radial flow decelerates rapidly. The decrease in radial inflow acts as a brake on the

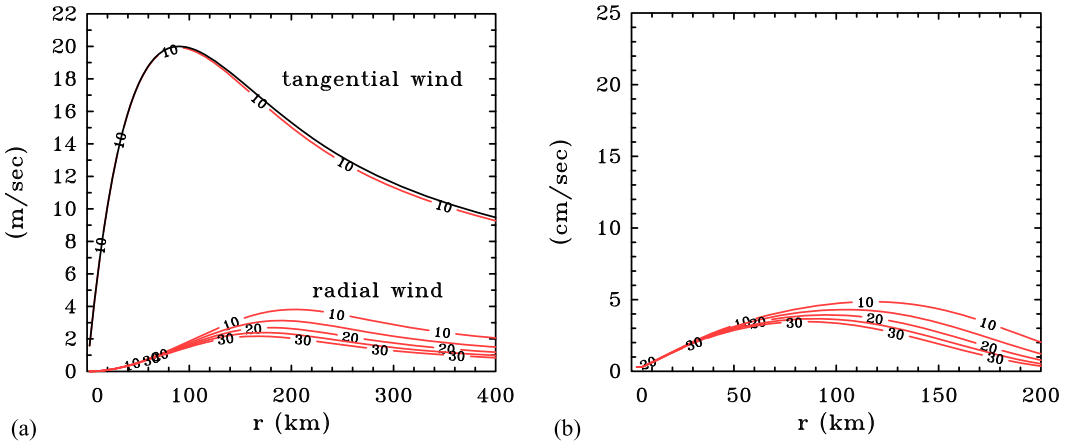

FIG. 3. (a) Radial profiles of radial and tangential wind components in the boundary layer for the linear solution given by Eqs. (10) and (11) for different values of latitude for a fixed profile of gradient wind at the top of the boundary layer (black line). (b) The corresponding profiles of vertical velocity at the top of the boundary layer [note the difference in the radial extent of the abscissa in (a) and (b)]. As in Fig. 2, the calculations are based on the assumption of a fixed boundary layer depth of 1 km.

continued increase[1] in v_b and leads also to a sharp increase in the vertical velocity at the top of the boundary layer (Fig. 2b). In the calculations shown, the radial inflow remains positive down to a radius of about 10 km, while inside the RMW the tangential wind in the boundary layer oscillates about the gradient wind. We do not attribute much significance to these oscillations in reality and, in fact, Kepert (2012) showed that they were an artifact of certain approximations made in deriving the slab model. For this reason, we do not give much weight to the solutions at inner radii where the oscillations occur.

Note that, as the latitude decreases, the maximum vertical velocity increases sharply, and its radial location moves inwards. The features described above are notable ones of the numerical model simulations discussed in the introduction and, with certain caveats discussed below, are suggestive that the behavior of the model simulations can be attributed to the dynamics of the boundary layer.

b. *Linear boundary layer approximation*

The foregoing features are mostly not found in the linear solution shown in Fig. 3. In this case, supergradient winds do not occur [a mere inspection of Eq. (11) shows that, in this solution, $v_b < v_g$ at all finite radii], and although the radial inflow increases with decreasing latitude, the radius of maximum inflow increases with decreasing latitude, a feature that has implications for the profile of vertical velocity at the top of the boundary layer (Fig. 3b). Note that the radius of the maximum vertical velocity increases with decreasing radius, unlike in the nonlinear case.

c. *Refinements to the slab boundary layer model*

There are several refinements that can be made to the constant-depth slab boundary layer model and some of these are discussed in appendix B. However, as shown there, the qualitative behavior of these refined models is similar to that described above, as is the broad dependence of the solutions on latitude.

d. *A question*

The initial vortices used in these calculations have a characteristic Rossby number ($\mathrm{Ro} = v_{\max}/fr_{\max}$) on the order of 3 or larger, where $v_{\max}$ is the maximum tangential wind and $r_{\max}$ is the radius of maximum tangential wind. Given the apparent subdominance of the planetary vorticity, a question arises as to why the vertical velocity exiting the boundary layer has such a large dependence on f. The answer is that, although the contribution of f to the total force balance is locally small compared with the other forces in the radial momentum equation within a few $r_{\max}$ of the center of circulation, the effect of f on the radial acceleration can be appreciable when the nonlinear radial momentum equation is integrated over a radial distance of several $r_{\max}$, as demonstrated above.

5. Discussion

The behavior of the steady, nonlinear, axisymmetric, slab boundary layer model as the latitude changes, even

[1] Mathematically, dividing Eq. (3) by u_b shows that the friction term is inversely proportional to u_b so that dv_b/dr is large and negative for small u_b. Physically, one may think of air parcels spiraling inwards, losing tangential momentum as they do so: the faster they move inward, the smaller the number of circuits in the spiral and therefore the smaller the effect of the frictional torque.

with a fixed profile of gradient wind above the boundary layer, is consistent with that in the three-dimensional MM5 calculations detailed in section 2 during the intensification phase and with the behavior in the models referred to in the introduction. In particular, the radial inflow increases in strength as the latitude in the model is decreased and the location of maximum inflow moves to a slightly smaller radius. Moreover, the maximum vertical velocity exiting through the top of the boundary layer increases significantly and its location moves also to a slightly smaller radius. As a result, it is tempting to attribute the behavior of the time-dependent models described in the introduction and in section 2 as the latitude is changed to the boundary layer dynamics. Here we explore a range of issues that complicate such an interpretation, focusing on the two calculations for 10° and 30°N.

a. *Steady-state issue*

First, we note that the boundary layer is a relatively thin layer driven by the radial pressure gradient just above it. Thus, it is reasonable to assume that to a first approximation the layer will respond rapidly to changes in the pressure gradient.

b. *Coupling issues*

It is important to bear in mind that the behavior of a tropical cyclone depends on a range of tightly coupled individual physical processes, both dynamical and thermodynamical. Even though these processes may be more or less well understood individually, understanding their tight coupling remains a challenge. Moreover, even though the slab boundary layer model is relatively simple, it does not seem possible to provide an intuitive explanation of why it behaves as it does: one has to perform nonlinear calculations to determine the behavior.

c. *Thermodynamic issues*

Even for a fixed profile of gradient wind, an increase in both the near-surface radial and tangential wind components at all radii in the boundary layer with decreasing latitude would imply an increase in surface evaporation at lower latitudes, at least if one assumes that the thermodynamic disequilibrium at the ocean–atmosphere interface is unchanged. This increase in surface evaporation is indeed the case in the experiments described in section 2, as shown in Figs. 4a and 4b.[2] It might be tempting to assume, as do Li et al. (2012), that the larger fluxes at low latitudes would lead to a larger amount of low-level moisture at these latitudes and hence to a larger amount of convective instability in the inner-core region of the nascent vortex. However, Figs. 4c and 4d show that this is not the case: on the contrary, the near-surface mixing ratio is marginally larger at 30° than at 10°N. The latter result may seem surprising, especially in view of the fact that the vertical velocity in the eyewall updraft is significantly larger at 10°N (Figs. 4e,f), suggesting a larger degree of convective instability at that latitude. However, it must be remembered that stronger convection will be accompanied by stronger downdrafts, which will tend to decrease the boundary layer moisture levels, especially during the early stages of vortex evolution when there is still dry air aloft.

d. *Convective instability issue*

One possible reason for the stronger updraft at 10°N might be a larger degree of convective instability as measured by the convective available potential energy (CAPE) and a smaller degree of convective inhibition (CIN). However, we know from the previous subsection that larger CAPE does not arise from an increase in the low-level moisture, so where would it come from? The answer could lie in the reduced upper-level stability associated with the low-latitude vortex. To illustrate this idea, we show in Figs. 5b–d the temperature anomaly at various latitudes of an idealized balanced vortex with the tangential wind distribution shown in Fig. 5a. For illustration, the tangential wind has a similar radial structure to the initial vortex in the MM5 calculations in section 2, with a maximum wind speed of 15 m s^{-1} at a radius of 100 km (in this case, taken at the surface). The wind speed declines sinusoidally with height, becoming zero at a height of about 16 km. The associated temperature anomalies at latitudes 10°, 20°, and 30°N show a temperature perturbation on the order of 1°C, the magnitude and radial extent of which increase with increasing latitude. The increased strength of the temperature anomaly with increasing latitude would imply a decrease in CAPE and an increase in CIN (Juckes and Smith 2000).

To check the foregoing ideas, we show in Figs. 6a,b and 6e,f Hovmöller diagrams of the CAPE and CIN, respectively, based on azimuthally averaged thermodynamic fields as a function of radius. The method used to calculate these quantities is explained in appendix C. In Fig. 6c, we show the difference between the two CAPE fields. Initially, there is no CAPE and significant CIN (reaching 180 J kg^{-1} at 10°N and 200 J kg^{-1} at 30°N), but CAPE is rapidly created by the surface moisture fluxes, and the CIN is rapidly reduced.

[2] Figure 4 shows the period of rapid intensification (RI) identified in Fig. 1. These periods occur when the maximum tangential wind speed increases by 3.75 m s^{-1} over a sustained period of 6 h, corresponding roughly with the definition of RI adopted by Kaplan and DeMaria (2003, p. 1098), who used the value of 30 knots (kt; 15.4 m s^{-1}) over 24 h.

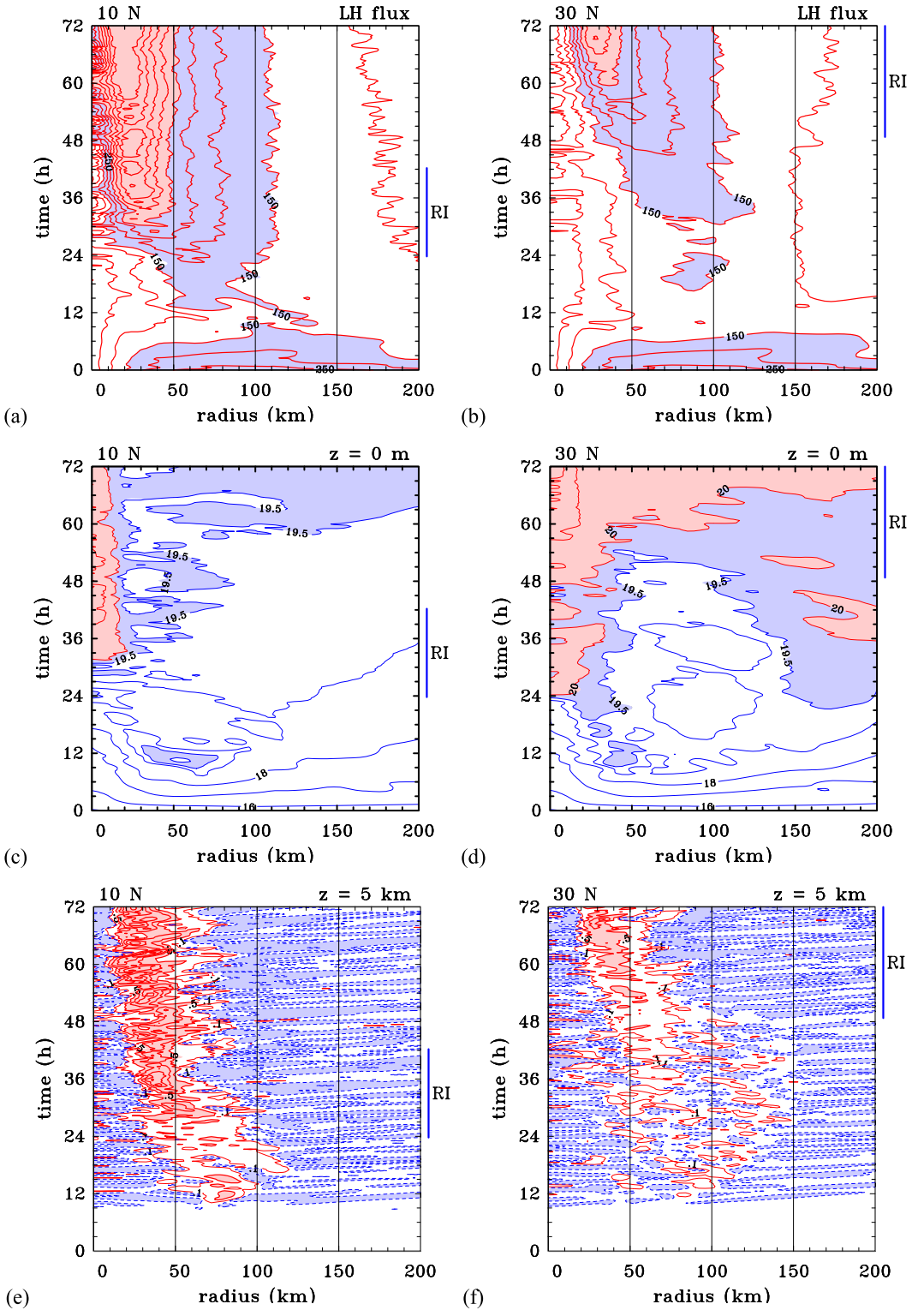

FIG. 4. Time–radius plots of azimuthally averaged surface latent heat fluxes in the MM5 calculations of section 2 at (a) 10° and (b) 30°N. (c),(d) The corresponding plots of specific humidity at the surface (0 m) and (e),(f) the contours of vertical velocity at a height of 5 km. Contour intervals in (a) and (b) are 50 W m^{-2}, values between 150 and 300 W m^{-2} are shaded light blue, and values $\geq$300 W m^{-2} are shaded pink. Contour intervals in (c) and (d) are 1 g kg^{-1}, values between 19.5 and 20 g kg^{-1} are shaded light blue, and values $\geq$20 g kg^{-1} are shaded pink. In (e) and (f), the interval for the thick solid contours is 0.5 m s^{-1} and values $\geq$0.5 m s^{-1} are shaded pink; the interval for the thin solid contours is 0.1 m s^{-1} and values ≤ -0.01 m s^{-1} are shaded light blue. The vertical line to the right of each panel shows the period of rapid intensification at the particular latitude (see Fig. 1).

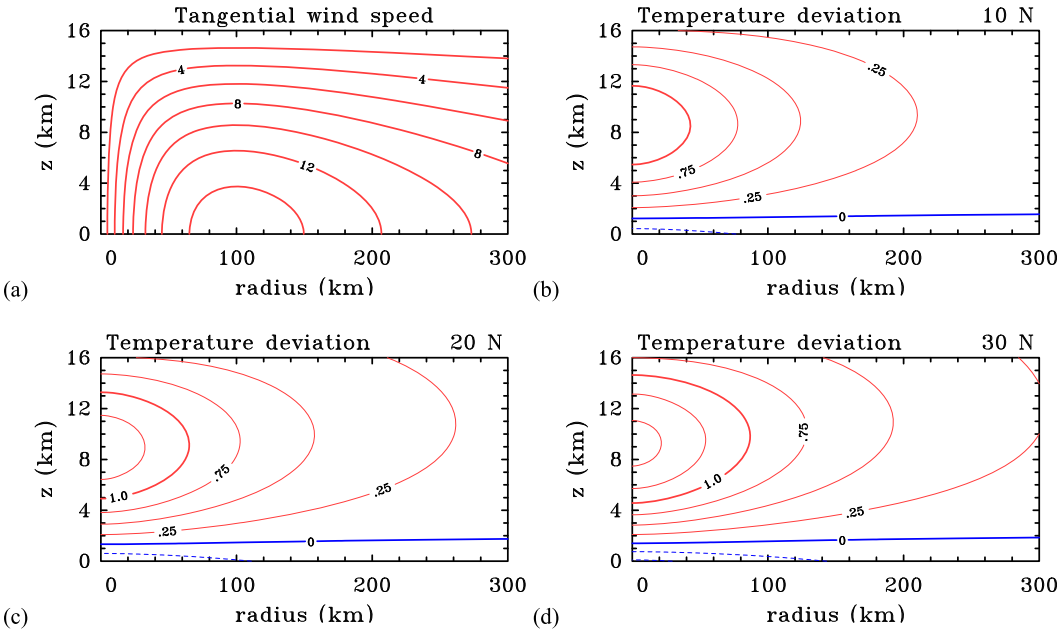

FIG. 5. Height–radius cross sections of (a) the tangential wind speed in the idealized warm-core vortex described in the text (contour interval: 2 m s^{-1}), and corresponding balanced temperature perturbations at (b) 10°, (c) 20°, and (d) 30°N (contour intervals: thick contours 1°C and thin contours 0.25°C). Solid (red) contours are positive, and dashed (blue) contours are negative.

At early times (between about 6 and 12 h, depending on the radius), the CAPE is larger in the 10°N calculation than in the 30°N calculation, as predicted above. Nevertheless, as deep convection develops, it consumes the low-level moisture as well as the CAPE so that the earlier onset of deep convection in the 10°N calculation leads to a reduction of surface moisture and CAPE compared with the 30°N calculation. This behavior is despite the fact that the surface moisture fluxes are higher in the 10°N calculation (Fig. 4) on account of the larger surface wind speeds (Fig. 1). However, as time proceeds, the larger consumption of CAPE by convection in the 10°N calculation leads to smaller values of CAPE than at 30°N after about 9–12 h, depending on the radius. This is about the time that convection begins to develop in both calculations (Fig. 6d), slightly later at 30°N on account of the larger initial CIN. These results indicate that the differences in CAPE and CIN between 10° and 30°N do not provide a robust explanation for the differences in the intensification rate between the two calculations.

e. *Diabatically forced overturning circulation*

In the context of axisymmetric balance dynamics, it is well known that a negative radial gradient of diabatic heating rate associated with deep convection will produce an inflow in the lower troposphere (Eliassen 1951; Willoughby 1979). This inflow is a feature of the conventional spin-up mechanism. In Figs. 7a and 7b, we show the distribution of azimuthally averaged diabatic heating rate $\dot{\theta}$ averaged over the period 14–16 h in the calculations for the two latitudes. This time range is a little after when convection is initiated in both calculations. It is clear that there is a large difference in the mean heating rates between the calculations in this time period, the maximum at 10°N being 26 K h^{-1}, compared with only 6 K h^{-1} at 30°N. Examination of the figure shows that the radial gradient of $\dot{\theta}$ is much larger at 10°N also. The larger gradient would be expected to lead to a much larger radial inflow, even if the latitudes were the same. Figures 7c and 7d show the isotachs of radial velocity in the balanced secondary circulation obtained by solving the Sawyer–Eliassen equation[3] for the initial vortex with one or the other of these heating rates as forcing and with the corresponding latitude. The streamfunction contours of this circulation are shown also. For simplicity, since the vortex is identical in both calculations (the same as that in the MM5 calculations in section 2), the frictional drag would be identical and therefore this drag is not included. Confirming expectations, the balanced secondary circulation is

[3] Specifically, we solve Eq. (14) of Bui et al. (2009), neglecting both frictional forcing and the relatively small contributions of the "eddy terms," as defined therein in this equation.

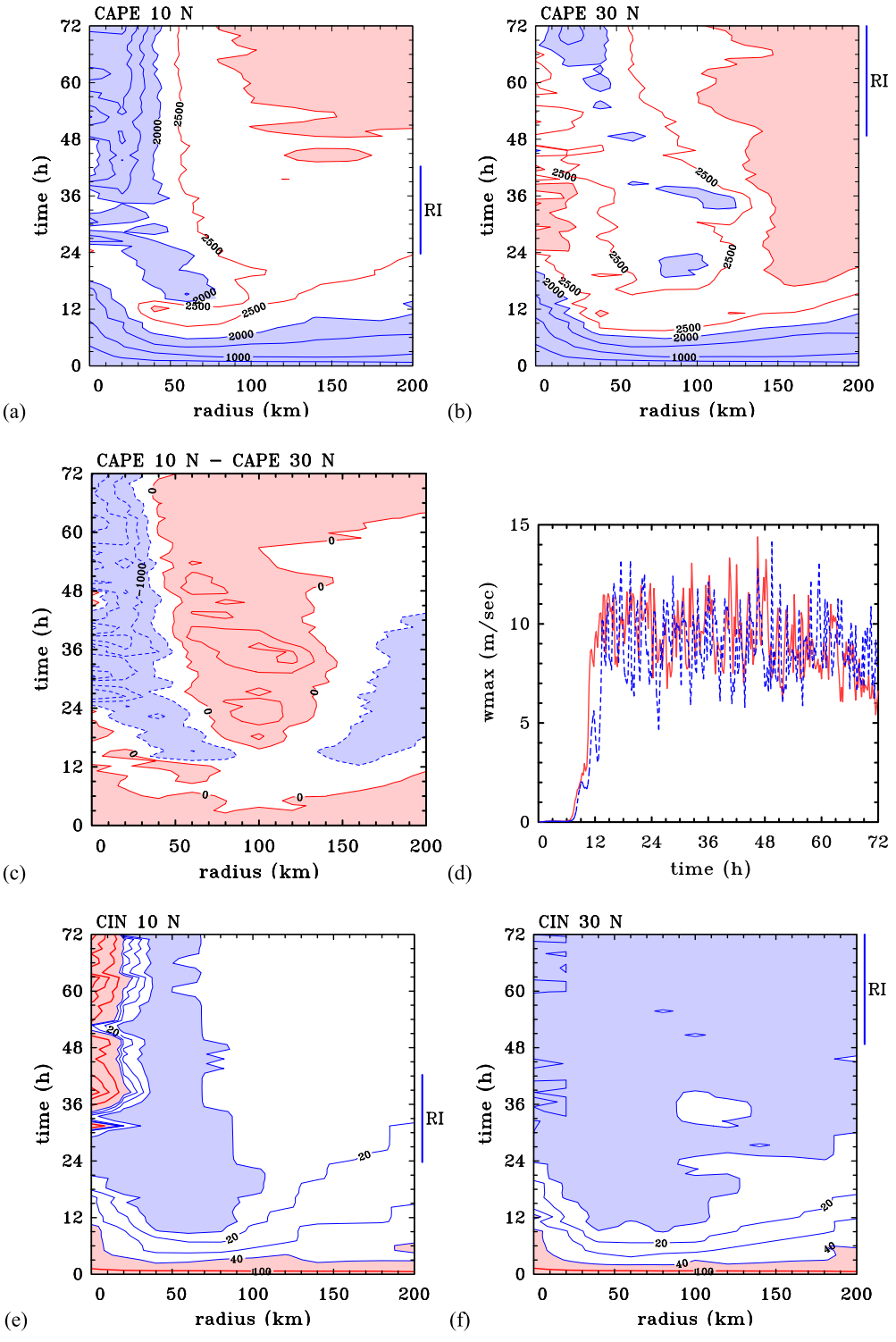

FIG. 6. Time–radius plots of CAPE based on azimuthally averaged thermodynamic data in the MM5 calculations of section 2 at (a) 10° and (b) 30°N; the contour interval is 500 J kg^{-1}, values below 2000 J kg^{-1} are shaded light blue, and values $\geq$ 3000 J kg^{-1} are shaded pink. (c) A similar plot of the difference in CAPE between these two calculations; the contour interval is 500 J kg^{-1}, values $\leq$ −500 J kg^{-1} are shaded light blue, and positive values are shaded pink. (d) A time series of the maximum vertical velocity (not azimuthally averaged) in the two calculations. (e),(f) The corresponding plots of CIN at 10° and 30°N, respectively (contours: 100, 40, 30, 20, and 10 J kg^{-1}). Regions of CIN with values < 10 J kg^{-1} are shaded light blue, and values > 40 J kg^{-1} are shaded pink. The vertical lines to the right of (a),(b),(e), and (f) show the period of rapid intensification at the particular latitude (see Fig. 1).

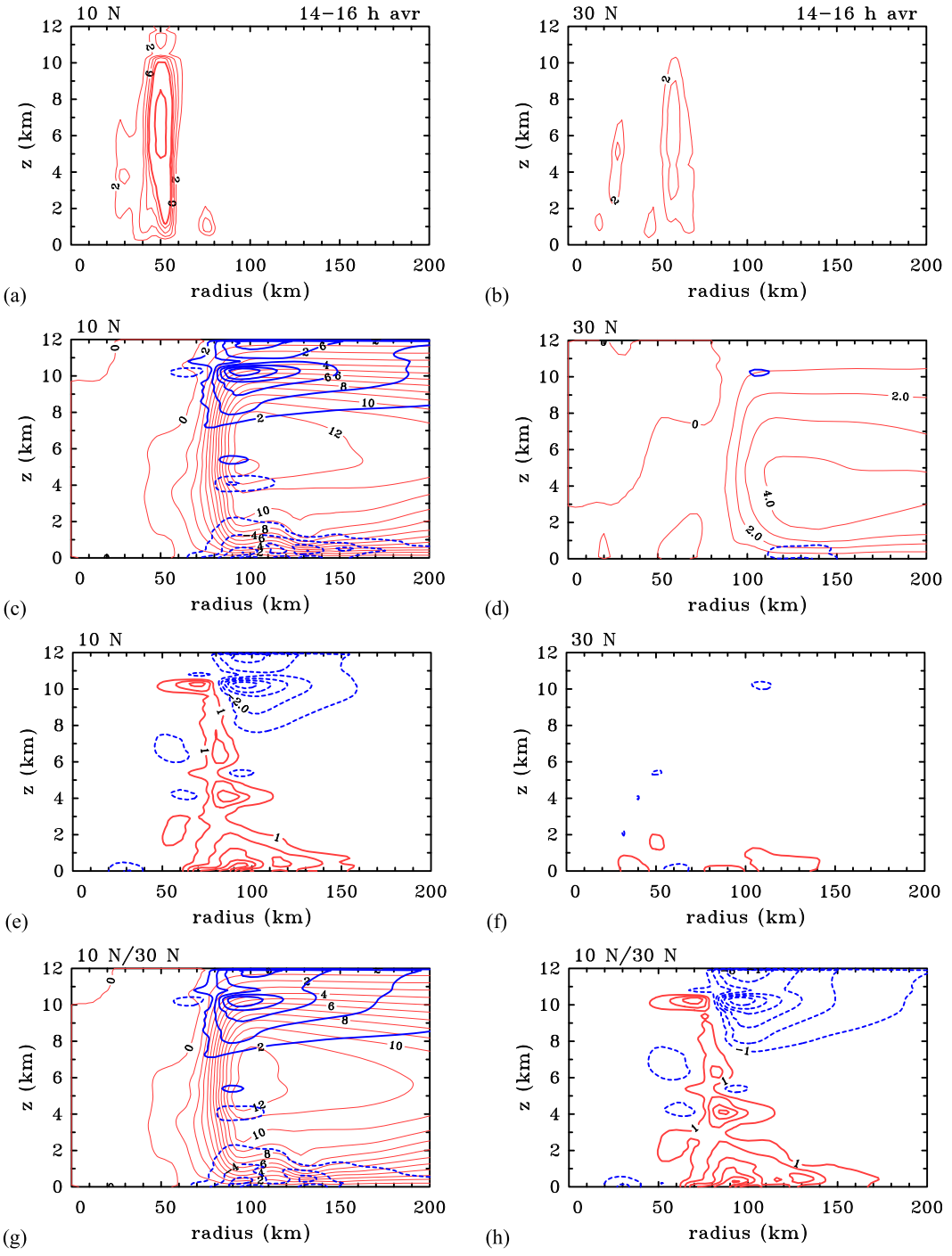

FIG. 7. Height–radius plots of the time-averaged diabatic heating rate for the period 14–16 h, based on azimuthally averaged fields from the MM5 calculations of section 2 at (a) 10° and (b) 30°N (contour intervals: thin contours 2 K h^{-1} and thick contours 10 K h^{-1}). (c),(d) The corresponding streamfunction of the balanced secondary circulation obtained by solving the Sawyer–Eliassen equation for the initial vortex with these heating rates as forcing (thin red contours, interval: 1×10^{-8} kg s^{-1}). Also shown are contours of the radial velocity component (thick blue contours, interval: 2 m s^{-1}; negative values dashed). (e),(f) The corresponding tendencies of the balanced tangential wind (contour interval: 1 m s^{-1} h^{-1}; positive values are solid red and negative values are dashed blue). (g),(h) The streamfunction and tendency when the Sawyer–Eliassen equation is solved for the 10°N heating rate in (a) at 30°N. These should be compared with (c) and (e), respectively.

much stronger in the 10°N calculation. In particular, the maximum inflow velocity is $8.1\,m\,s^{-1}$, compared with only $2.5\,m\,s^{-1}$ in the 30°N calculation.

Since we have shown that the CAPE is only fractionally larger at early times in the 10°N calculation (no more than about $50\,J\,kg^{-1}$), the large difference in diagnosed heating rates, which are closely tied to the vertical velocity (Holton 2004), cannot be explained in terms of differences in updraft buoyancy. The explanation for this difference must be attributed either to the difference in the vertical velocity at the top of the boundary layer or to the effects of rotational stiffness above the boundary layer,[4] which would suppress the inflow and thereby, through continuity, inhibit the vertical velocity.

f. Rotational stiffness

Basic fluid-dynamical considerations would suggest that the ability of deep convection to draw air inward above the boundary layer is constrained by the rotational stiffness of the vortex, as quantified by the inertial stability I^2, defined in section 3. For a cyclonic vortex, this quantity increases with latitude through its dependence on f. Accordingly, for a fixed distribution of diabatic heating rate and for the same initial vortex, there must be stronger inflow at lower latitudes. However, if the Rossby number is order 1 or greater, this effect should not be large and would seem unlikely to be able to explain the significant difference in diabatic heating rates and associated radial gradients reported above. To test this expectation, we show in Fig. 7g the secondary circulation at 30°N, but with the diabatic heating rate at 10°N, allowing us to isolate the effect of rotational stiffness. As anticipated, there is only a small reduction in the maximum inflow velocity from 8.1 to $7.1\,m\,s^{-1}$ (i.e., less than about 13%).

The reduced inflow with increasing latitude will not necessarily lead to slower spinup, because the tendency of the tangential wind on account of radial influx of absolute vorticity is the product of the inflow velocity and the absolute vorticity, but the latter increases with increasing latitude. Basically, one has to do the calculation to determine the net effect on the tangential wind tendency.

Isotachs of the tangential wind tendency at 10° and 30°N for the two calculations with different heating rates and that for the calculation at 30°N with the same heating rate as at 10°N are shown in Figs. 7e, 7f, and 7h, respectively. Comparing Figs. 7e and 7f, in which both Coriolis parameter and heating rates change, shows a much larger positive tendency at 10°N ($5.6\,m\,s^{-1}\,h^{-1}$ compared with $1.7\,m\,s^{-1}\,h^{-1}$ at 30°N). However, for the same heating rate (i.e., at 10°N), the differences are small (cf. Figs. 7e and 7h), but the inviscid tendency at 30°N is actually slightly larger ($6.2\,m\,s^{-1}\,h^{-1}$) than that at 10°N ($5.6\,m\,s^{-1}\,h^{-1}$). Taken together, these results demonstrate that the difference in intensification rates in the two MM5 calculations cannot be attributed to the larger inertial stability at the higher latitude, leaving the difference in the heating rates and associated radial gradients as the culprit.

g. Ooyama's linear model predictions

As noted in the introduction, Ooyama (1969) presented a linearized version of his axisymmetric cooperative intensification model, in which the growth rate [his Eq. (8.10)] of a small-amplitude initial disturbance was shown to increase with decreasing latitude. This growth rate is linearly proportional to the drag coefficient and a quantity that is the ratio of two terms. The numerator in this ratio is a measure of the degree of convective instability tempered by a term that represents the size of the convective region relative to the internal Rossby length; the denominator is a monotonically increasing quadratic polynomial of this term. From the formula, it follows that the growth rate decreases with increasing latitude. In the linear version of the model, the convection is represented by an entraining plume model in which the mass flux is simply proportional to the upward vertical velocity at the top of the boundary layer and the entrainment into the plume is proportional to the mass flux itself and to the degree of convective instability, which is constant in the linear model. The entrainment leads to system-scale inflow that draws absolute angular momentum surfaces inward to spin up the vortex. The vertical velocity at the top of the boundary layer is determined on the basis of an Ekman-like balanced boundary layer calculation (Smith and Montgomery 2008) and, for a fixed radial profile of tangential wind, varies inversely with latitude. In essence, for a fixed degree of convective instability, the magnitude of the effective diabatic heating and its radial gradient are controlled by the dynamics of the boundary layer and, in particular, on the latitude.

Although Ooyama's linearized model exhibits a qualitatively consistent dependence of the growth rate with latitude as found in the MM5 calculations, the linearized model is highly simplified, and the validity of the cumulus parameterization in the linear realm with no mean vortex

[4] Since the frictional reduction of the tangential wind speed leads to a net inward radial force in the boundary layer, except possibly near and inside the radius of maximum tangential wind speed, the concepts of inertial stability or rotational stiffness within the boundary layer in terms of a force-resisting motion would seem to be inapplicable.

is questionable [see Ooyama (1982) for details]. Another limitation of the Ooyama model is that the formulation is strongly dependent on the cumulus convection parameterization, which ties the convective mass flux to the frictional mass convergence. Since the Ooyama (1969) model assumes that the tangential wind in the boundary layer is equal to the gradient wind in the middle layer, it follows that the model precludes also the boundary layer spin-up mechanism outlined in the introduction.

Craig and Gray (1996) critiqued the Ooyama (1964, 1969) theories and the corresponding conventional spin-up mechanism therein based on the fact that the spin-up rate in the axisymmetric Rotunno and Emanuel (1987) model did not increase with increasing drag coefficient, in contradiction to Ooyama's linear growth rate formula [his Eq. (8.10)]. Craig and Gray's results were refuted by Montgomery et al. (2010) and Persing et al. (2013) for realistic forecast time scales using two independent three-dimensional near-cloud-resolving numerical model frameworks and consistent physical interpretations based on the boundary layer dynamics of the system-scale vortex. Persing et al. (2013) highlighted also fundamental differences between tropical cyclone intensification in strictly axisymmetric and three-dimensional configurations and showed that, in the three-dimensional configuration, the convective organization in azimuth is fostered by surface friction. Thus, despite the caveats associated with the Ooyama's linearized model, it appears to capture several of the physical elements identified here in the azimuthally averaged view of the problem using MM5.

h. Summary

As noted at the beginning of this section, comparison between the steady, slab boundary layer model and the time-dependent numerical solutions discussed in sections 4 and 2 is suggestive that the boundary layer is a key element in the latitudinal dependence of the intensification rate in the numerical simulations. We have explored a range of effects that may also be elements of the interpretation. These include the differences in surface evaporation, differences in CAPE, differences in the magnitude and structure of the diabatic heating rate, and the effects of rotational stiffness. In an azimuthally averaged view of the problem, the most prominent quantitative difference between the time-dependent simulations at 10° and 30°N is the much larger diabatic heating rate and its spatial gradient above the boundary layer at the lower latitude. We attribute these differences in heating rate to the larger vertical velocity found through the troposphere at 10°N, because the heating rate itself is approximately proportional to the vertical velocity.

We showed that the differences in moisture fluxes and CAPE are relatively small between the two simulations, as is the difference in the balanced overturning circulation (for a fixed distribution of diabatic forcing), as the rotational stiffness is varied. It follows that the differences in the vertical velocity must be due primarily to the differences in vertical velocity exiting the boundary layer.

Recall that the spatial gradient (primarily the radial gradient) of the heating rate is the forcing term for the low- and midtropospheric radial inflow, thereby determining the rate at which absolute angular momentum surfaces are drawn inward. Although the radial gradient of M is larger at 30° than at 10°N, significantly larger at outer radii, the much larger inflow at 10°N is sufficient to give the larger spin-up rate at this latitude. Thus, the much larger diabatic forcing at 10°N leads to a more rapid spinup than at 30°N.

This interpretation invokes the conventional spin-up mechanism as discussed in the introduction together with a boundary layer feedback mechanism linking the strength and location of the boundary layer inflow to that of the diabatic forcing. While the boundary layer spin-up mechanism is operative in the numerical model calculations, our interpretation here does not call on this aspect qualitatively inasmuch as it affects v_{max} to explain the dependence of the intensification rate on latitude. However, as shown in the slab boundary layer solutions in section 3 and the more sophisticated ones in appendix B, the nonlinear terms in the boundary layer formulation amplify the rate of mass convergence in the boundary layer as the latitude is decreased and lead to a contraction in the radial position of the maximum inflow (see Figs. 2a and 3). The latter feature is not captured in a quasi-linear (Ekman) slab boundary layer formulation for a fixed gradient wind at the boundary layer top.

In both calculations, there appears to be an adequate moisture supply to maintain convective instability during the intensification phase, providing sufficient local buoyancy in the inner core of the vortex to loft the mass that converges in the boundary layer to the upper troposphere.

i. Nonaxisymmetric issues

At this stage, the explanations of the higher rate of intensification at low latitudes have been based on axisymmetric concepts. However, as in previous studies (e.g., Nguyen et al. 2008; Fang and Zhang 2011; Gopalakrishnan et al. 2011; Persing et al. 2013), the flow evolution during the process of intensification is distinctly nonaxisymmetric, with rotating convective structures and their progressive aggregation being a dominant feature. In fact, during the intensification

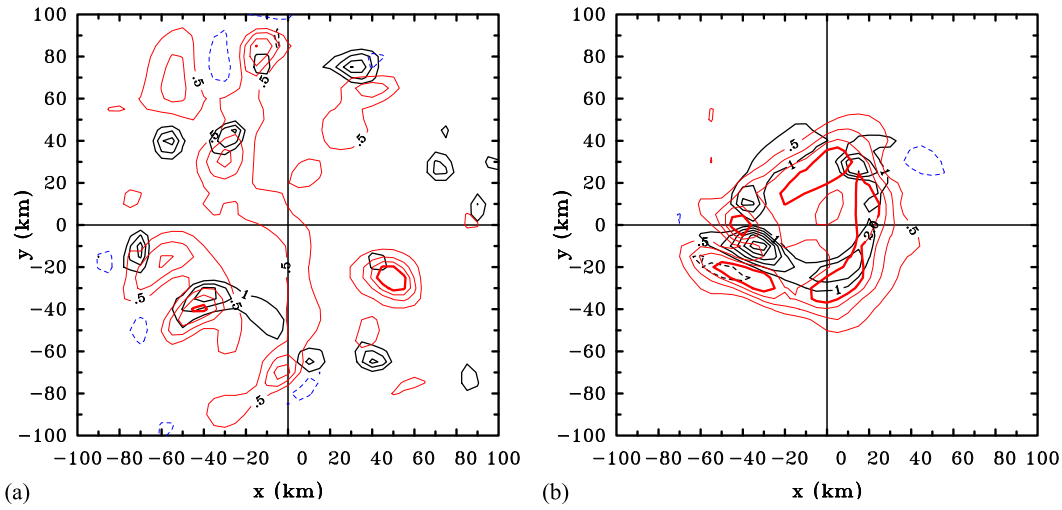

FIG. 8. Horizontal cross sections of vertical velocity (black contours) and vertical relative vorticity (positive values are red; negative values are blue) at a height of 5 km in the 10°N calculation at (a) 24 and (b) 36 h. Contour interval for vertical velocity (black): 1 m s^{-1}; solid contours are positive and dashed contours are negative. Contour intervals for vertical vorticity: thin contours 5×10^{-4} s^{-1} from 5×10^{-4} to 1.5×10^{-3} s^{-1} and thick contours 2×10^{-3} s^{-1}. Solid (red) contours are positive, and dashed (blue) contours are negative.

phase, the azimuthally averaged fields of vertical velocity, vertical vorticity, and diabatic heating rate are dominated by these local features. In other words, the mean flow is dominated by these localized coherent structures. Presumably then, these eddy processes should figure prominently in a complete dynamical explanation of the phenomenon (Persing et al. 2013).

To illustrate these nonaxisymmetric features, Fig. 8 shows vertical velocity and relative vorticity at 5-km height for the 10°N experiment at 24 and 36 h. At 24 h, the vortex is just beginning to intensify (Fig. 1a), and the vertical velocity field consists of a few isolated convective towers, with nearby patches of mainly cyclonic relative vorticity. At 36 h, which is beyond the middle of the rapid intensification period (see Fig. 1a), the vorticity and vertical velocity have consolidated to some degree but exhibit significant asymmetry. Plots for 30°N are qualitatively similar, but the intensification process proceeds more slowly, and the vorticity structures consolidate some 18–20 h later compared to the 10°N experiment.

6. Previous explanations and appraisal

In this subsection, we summarize prior studies (excluding those discussed in the introduction) that examined the dependence of the intensification and mature intensity on latitude. Then, using the results and insights developed in the foregoing sections, we offer an appraisal of previous explanations of the dependence of spinup on latitude.

a. DeMaria and Pickle

Using an idealized, axisymmetric, three-layer model, DeMaria and Pickle (1988) found that low-latitude storms are smaller than high-latitude storms, but these storms intensify more rapidly initially than those at higher latitudes. In addition, they showed that the final intensity of storms does not vary appreciably (they say "rapidly") with latitude. These authors wrote that "the effect of latitude appears to be related to the radial positioning of the diabatic heating" and argued that "the boundary-layer convergence and thus the diabatic heating occur much closer to the storm centre as the latitude is decreased" (p. 1554). To explain the link between the diabatic heating and the boundary layer convergence, as well as the dependence of the intensification rate with latitude, they wrote, "In this model, the radial structure of the diabatic heating is controlled by the evolution of the boundary layer convergence" (p. 1549). Our findings support the idea that the radial positioning of the diabatic heating is linked to that of the boundary layer convergence. However, our results (see section 5e) underscore also the role of the boundary layer convergence in regulating the magnitude of the diabatic heating rate and, in turn, the convectively induced convergence of absolute angular momentum above the boundary layer (the conventional spin-up mechanism discussed in the introduction).

DeMaria and Pickle (1988) go on to say, "One factor which affects the boundary layer convergence is *the magnitude of the Coriolis force*. At low latitudes *the air in the boundary layer is able to penetrate closer to the*

storm center before it is deflected by the Coriolis force, so the diabatic heating should occur closer to the storm center'' (p. 1549; emphasis added). Although this explanation seems plausible at first sight, it is incomplete. It is not the Coriolis force per se that produces the deflection. The material deflection of an air parcel from the radial to the tangential direction depends on the generalized Coriolis force, $-u(v/r + f)$, and the frictional force [see Eq. (3)]. Furthermore, the air is not suddenly deflected after it penetrates to the central region. In fact, the Coriolis force acts progressively on fluid parcels, as do the centrifugal and frictional forces. Moreover, as we have shown in section 3, the nonlinear accelerations need to be included in the explanation.

b. *Rappin et al.*

Rappin et al. (2011) carried out two simulations in a quiescent environment, one at 10°N, the other at 30°N. They hypothesized that ''by reducing the angular momentum of the environment around numerically simulated tropical cyclones to a value close to that of typical outflow values, the tropical cyclone will undergo symmetric intensification more quickly and reach maximum intensity sooner'' (p. 179, left column). Here, outflow refers to the upper-tropospheric outflow of the storm. They found that the 10°N simulation ''exhibits a strongly divergent outflow initially, which subsequently weakens, while the 30°N simulation displays a slow, near-linear increase of divergent outflow in time.'' They argued that ''the smaller Rossby radius of deformation of the 30°N simulation leads to rotational flow closer to the storm core than in the 10°N simulation and the development of an intense, symmetric, anticyclonic jet. Then, as the outflow expands, there is a loss of the divergent (i.e., radial) wind at the expense of rotational (i.e., tangential) wind'' (p. 181, left column). Borrowing from ''work concepts'' used in the Carnot cycle theory for hurricane maximum intensity (Emanuel 1986), Rappin et al. (2011) offered an interpretation of their findings based on the work done in the outflow and ''the energy expended by the hurricane to spin up and expand the outflow anticyclone.'' They stated, ''with weak inertial stability, the environment provides little resistance to being pushed aside, leading to more rapid intensification'' (p. 181, right column and accompanying discussion).

We have a number of concerns about the foregoing arguments. First, it is unclear that more work is done by the upper anticyclone at higher latitudes as the Coriolis force, being normal to the wind vector, does no work;[5] therefore, the Coriolis parameter (and indeed the generalized Coriolis terms in the horizontal momentum equations in cylindrical coordinates) does not appear in the energy equation. It is true that some of the energy expended by a storm must go into spinning up the upper anticyclone. However, because the upper anticyclone is more confined at higher latitudes and the Coriolis force in the radial momentum equation opposing its outward spread is larger, the argument as it affects the strength of convection is incomplete unless it is demonstrated that the total kinetic energy of the larger and weaker anticyclone at low latitudes is less than that of the anticyclone at higher latitudes.

A second concern we have is that, while the inner-core vortex intensity reaches a quasi-steady state after about 60 h, the upper anticyclone may still be evolving, as, for example, in the calculations of Smith et al. (2014).

A third concern we have is that Rappin et al.'s (2011) arguments are focused predominantly on the upper-tropospheric outflow layer, maintaining that it is the inertial stability of the upper troposphere that is decisive. However, we have shown above that the inertial stability effect is less important than the differences in the azimuthally averaged diabatic heating rate and the corresponding spatial gradients.

Finally, their arguments ignore altogether the boundary layer dynamics, which we have shown to be the most important regulator of the diabatic heating rate.

c. *Li et al.*

As noted earlier, Li et al. (2012) implicate the role of unbalanced effects in the boundary layer. They say, ''Given an initial balanced vortex, surface friction destroys the gradient wind balance, leading to subgradient inflow in the boundary layer. The friction induced inflow is stronger and deeper under lower planetary vorticity environment [*sic*], which brings about greater moisture convergence and leads to greater condensational heating in the TC [tropical cyclone; our insertion] core region. The strengthened heating lowers the central surface pressure, which further enhances the radial inflow. Through this positive feedback loop, the vortex spins up at a faster rate under lower planetary vorticity environment'' (p. 251). Elsewhere, they state that ''the strengthening of the radial inflow accelerates the development of local vorticity (and thus tangential wind) through a vorticity stretching effect'' (p. 244).

Many of the details of the purported positive feedback loop are unclear to us: for example, they do not explain why the boundary layer inflow in their model is deeper and stronger at lower latitudes (see their Fig. 8); they do not explain how ''greater condensational heating'' leads to a lower central surface pressure; and they do not say

[5] Indeed, this fact is consistent with their expression for work in their equation on page 182, since f vanishes on substitution for M.

how *radial inflow* leads to the amplification of vorticity (presumably vertical vorticity) by stretching, nor how the amplified vorticity generates increased circulation at a given radius.[6] In particular, Li et al. (2012) do not say whether their finding that ''the friction induced inflow is stronger and deeper under lower planetary vorticity environment'' is a result of boundary layer dynamics or of the ''greater condensational heating'' that occurs above the boundary layer.

7. Conclusions

We have examined why model tropical cyclones intensify more rapidly at low latitudes. After considering a range of physical processes involved in the intensification of storms, our analysis indicates that the dynamics of the frictional boundary layer is a key element.

To help isolate the effect of the boundary layer, we examined first a steady slab boundary layer model. This model provides a useful starting point for understanding the dependence of the spin-up rate on latitude. This is because it replicates some essential structural features of many previous studies and of new, three-dimensional, time-dependent numerical simulations for the prototype intensification problem in a quiescent environment. In particular, despite the steady-state restriction, the slab model produces stronger low-level inflow and stronger and more confined ascent out of the boundary layer as the latitude of the calculation is decreased, even if the tangential wind profile at the top of the boundary layer is held fixed. The ramifications of these and other features on various mechanisms in the time-dependent numerical simulations have been explored.

In an azimuthally averaged view of the problem, one of the most prominent quantitative differences between the time-dependent simulations at 10° and 30°N is the much larger diabatic heating rate and its radial gradient above the boundary layer at 10°N. We attribute these differences in heating rate to the larger vertical velocity found through the troposphere at 10°N, because the heating rate itself is approximately proportional to the vertical velocity. Since the differences in CAPE are found to be relatively small between the two latitudes at early times, the differences in the vertical velocity must be due to the differences in vertical velocity exiting the boundary layer. The much larger radial gradient of diabatic heating at 10°N produces a larger radial inflow in the low and midtroposphere, leading to an increase in the rate at which absolute angular momentum surfaces are drawn inwards. Although the radial gradient of M is larger at 30° than at 10°N, the much larger inflow at 10°N is sufficient to give the larger spin-up rate at this latitude.

These arguments for the dependence of spin-up rate on latitude invoke the conventional spin-up mechanism, as discussed in the introduction, together with a boundary layer feedback mechanism linking the strength of the boundary layer inflow to that of the diabatic forcing. The foregoing differences greatly surpass the effects of rotational stiffness (inertial stability) and evaporative-wind feedback that have been proposed in some prior explanations.

Since the azimuthally averaged fields of vertical velocity, vertical vorticity, and diabatic heating rate are found to be dominated by localized, rotating convective structures and their progressive aggregation, a more complete understanding of the dependence of latitude on the intensification problem requires an improved understanding of the influence of ambient rotation on these localized structures and their coupling to the boundary layer and interior vortex.

Acknowledgments. We are grateful to Dr. Gerald Thomsen, who set up the numerical calculations that form the basis of section 2. This paper was completed during a productive and enjoyable visit to the Bureau of Meteorology's Regional Forecasting Centre in Darwin, Australia, in January 2014, and we thank Andrew Tupper and Todd Smith for hosting our visit and providing a stimulating atmosphere for conducting our research. RKS and GK acknowledge financial support for this research from the German Research Council (Deutsche Forschungsgemeinschaft) under Grant SM30-23. MTM acknowledges the support of NSF AGS-0733380, NASA Grant NNG11PK021, and insightful email correspondence in 2011 with Dr. F. Fendell regarding the Carrier theory of tropical cyclone intensification. The authors thank also Dr. S. Abarca for his assistance in streamlining the numerical code to solve the Sawyer–Eliassen balance equation developed earlier by RKS, MTM, and Dr. Hai Bui. Finally, we thank John Molinari and Dave Raymond for their perceptive comments on the manuscript.

APPENDIX A

Some Remarks on the Slab Model

Some might object that the simple slab boundary layer used herein is too inaccurate and the fact that the

[6] Stretching of vorticity, by itself, accompanied by a reduction in the areal distribution of vorticity does not lead to increased circulation about a fixed circuit (Haynes and McIntyre 1987). In the absence of tilting, there must be a net influx of absolute vorticity into the circuit in order to increase the absolute circulation at a given radius.

solution breaks down when the radial motion becomes zero, or that the solution oscillates about the gradient wind, is physically unrealistic. Despite these limitations, we would argue that the model contains the essential physics to represent the processes that are germane to the qualitative arguments presented above. The inner-core breakdown of the slab model is of no consequence for these arguments. Kepert (2010) wrote a useful summary of the potential inaccuracies of the slab boundary layer, comparing the predictions of such models with a more sophisticated boundary layer model that goes some way to resolving the vertical structure of the boundary layer. As discussed by Smith and Montgomery (2010), there are serious mathematical issues with the more sophisticated model in that it requires a specification of both the radial and tangential wind components at the top of the boundary layer where the flow exits the boundary layer. Despite the claims by Kepert (2010, p. 1689) that he did not apply such a boundary condition but rather zero vertical gradient condition, it was shown by Smith and Montgomery (2010) that the zero-gradient boundary condition is equivalent to the imposition of a prescribed flow in gradient wind balance with effectively zero radial inflow. For this reason, we consider such comparisons to be problematic. It turns out that the specification of an upper boundary condition on velocity is not required to solve the slab model where there is ascent out of the boundary layer, and in this respect the slab model is superior to the more sophisticated one. Some issues with regard to the imposition of a prescribed time-independent flow at the top of the boundary layer may be inferred from recent results of Rotunno (2014) for a swirling boundary layer below a Rankine vortex. This flow has a propensity to undergo vortex breakdown, in which the upflow out of the boundary layer exhibits a centrifugal "jump" accompanied by centrifugal (inertial) waves over some appreciable depth of the vortex. Given this behavior, it is generally not possible a priori to specify the tangential wind at some prescribed height. Numerical solutions of tropical cyclones exhibit a similar behavior (Smith et al. 2009; Bryan and Rotunno 2009; Persing et al. 2013).

APPENDIX B

Some Refinements of the Slab Model

a. Variable-depth boundary layer

Although many previous studies have employed the simplification of a constant-depth boundary layer, the approximation is not supported by a scale analysis of the boundary layer equations, at least if the vertical eddy diffusivity K is assumed constant (e.g., Vogl and Smith 2009). The scale analysis shows that for constant K, the boundary layer depth decreases as the square root of the inertial stability $I^{-1/2}$ increases. It is easy to incorporate this behavior into the slab model, since the depth h in Eqs. (2) and (3) is purely parametric. However, the radial variation of h modifies the calculation of w_h in Eq. (5), requiring an additional term, $-(u_b/h)dh/dr$, to be inserted in the curly brackets. Of course, the model still requires the specification of h at large radius. The solution with this depth variation included is shown in Figs. B1a and B1b, with the value of h at large radius (1000 m), as in the calculations above. Comparing Figs. B1a and B1b with Figs. 2a and 2b shows that, for a given latitude, the reduction of boundary layer depth with increasing inertial stability of the gradient wind has a significant impact on the solutions. The reduction increases the effective drag (C_D/h), which typically reduces v_b, increasing the effective net inward pressure gradient force $(v_g^2 - v_b^2)/r + f(v_g - v_b)$, thereby increasing the radial acceleration. Thus, u_b becomes significantly larger than in the case of fixed boundary layer depth. However, it turns out that the larger inflow is opposed by the reduction in boundary layer depth to the extent that the inward volume flux is actually reduced (not shown). As a result, values of w_h are reduced in comparison with those in Fig. 2. As seen in Fig. B1, the effects of variable depth become more pronounced as the latitude decreases. Note, as a result of v_b decreasing with decreasing latitude, the radius at which v_b first exceeds v_g becomes smaller and, as a result, there is little difference in the maximum magnitude of v_b as the latitude changes. The most significant changes are in the secondary circulation induced by the boundary layer.

b. Boundary layer depth varying with latitude

Based on the results of Li et al. (2012) and our own calculations described in section 2, one might object that the foregoing calculations neglect the possible latitudinal differences in the boundary layer depth at large radii, which an Ekman-layer scaling shows to vary as $\sqrt{2K/f}$, where K is a scale for the vertical eddy diffusivity (e.g., Vogl and Smith 2009). To show the effect of this variation, we compare in Figs. B1c and B1d the solutions for u_b, v_b, and w_b for a boundary layer with the same gradient wind profile used in the calculations for Figs. 2 and 3, where the boundary layer depth is allowed to vary with radius as before, but where the depth at large radius is equal to $1000 \times \sqrt{f_{20}/f}$ m, where f_{20} is the value of the Coriolis parameter at 20° latitude. The solutions are qualitatively similar to those in

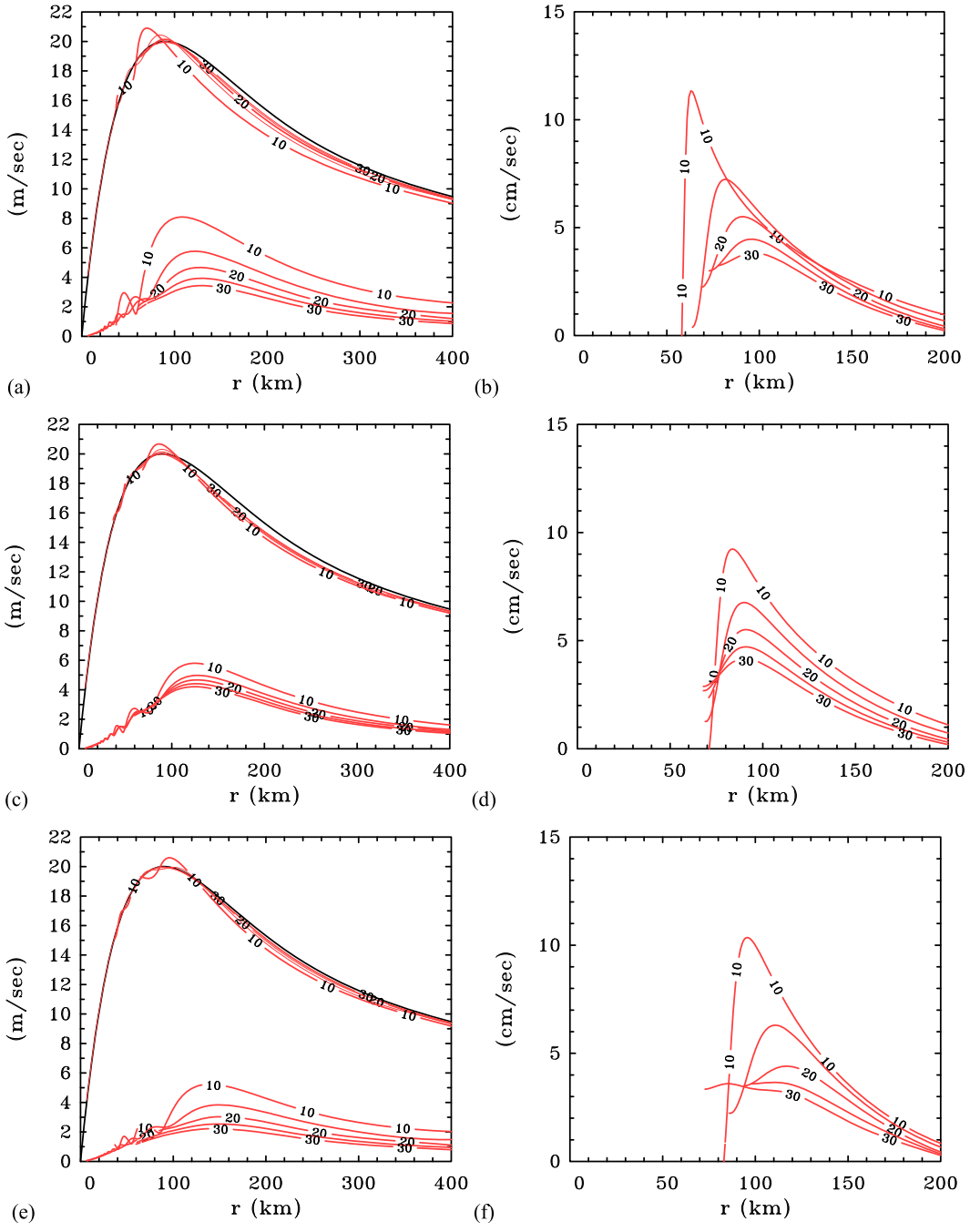

FIG. B1. Radial profiles of (a),(c),(e) radial and tangential wind components in the boundary layer and (b),(d),(f) upward vertical velocity at the top of the boundary layer for different values of latitude and for a fixed profile of gradient wind at the top of the boundary layer [black line in (a),(c), and (e)]. Note the difference in the radial extent of the abscissa in the two columns. In all cases, the boundary layer depth varies with radius inversely proportion to $I^{-1/2}$. (a),(b) The solutions in which the boundary layer depth at large radius is 1 km; (c),(d) the case where the depth at large radius is $1000 \times \sqrt{f_{20}/f}$ m; and (e),(f) as in (c) and (d), respectively, except where the effective eddy diffusivity increases in proportion to the gradient wind speed.

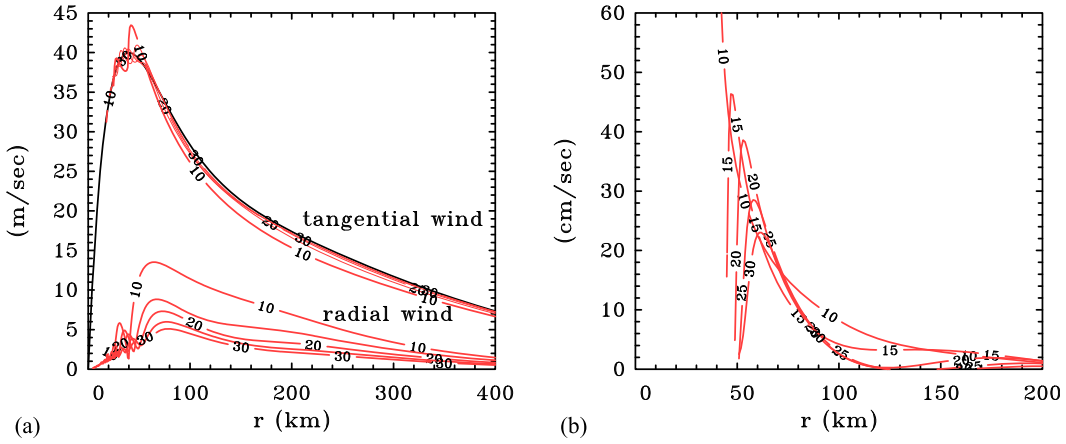

FIG. B2. As in Figs. 4e and 4f, but with a stronger and more peaked gradient wind profile at the top of the boundary layer. In these calculations, the effective eddy diffusivity increases linearly as the radius decreases.

Figs. B1a and B1b, but the latitudinal differences are less pronounced than in the case of where the depth at large radius does not vary with latitude. The maximum tangential wind speed in the boundary layer increases only slightly with decreasing latitude, a result that may be expected, since, as explained in section a, when v_b becomes supergradient, the radial flow slows down rapidly, leading to a rapid slowdown in the increase in v_b.

c. *Increased vertical mixing at stronger wind speeds*

The numerical calculations of Braun and Tao (2000) and Smith and Thomsen (2010), which include boundary layer schemes with different degrees of sophistication, show that the vertical eddy diffusivity increases as the wind speeds become stronger, an effect that would mitigate the decrease in boundary layer depth because of the increase in the inertial stability parameter. Indeed, this increase in K would explain why the inflow depth shown in Figs. 1e and 1f appears to increase with decreasing radius as the RMW is approached. To assess the impact of a radially varying K on boundary layer depth in the context of the present calculations, we carried out a calculation similar to that described in section 7, in which we allowed the depth to increase in proportion to $\sqrt{v_g/v_g(R)}$, where $v_g(R)$ is the value of the gradient wind at the starting radius. The results are shown in Figs. B1e and B1f. Broadly speaking, the only appreciable difference in the solutions is the slight reduction in the inflow velocity and the degree of gradient wind imbalance in the boundary layer outside of the RMW (resulting from an effectively deeper boundary layer) and a slightly outward location of the maximum updraft compared with the case of eddy diffusivity (cf. Figs. B1f and B1d).

d. *Stronger vortex*

To demonstrate that a similar behavior of the boundary layer with changing latitude occurs for more compact gradient wind profiles with larger wind maxima, more typical of moderate strength hurricanes, we show in Fig. B2 the corresponding profiles to those in Figs. B1e and B1f, but for a calculation with the gradient wind given by Eq. (12) that has a maximum wind speed of 40 m s^{-1} at a radius of 40 km and a radius of gale-force winds (17 m s^{-1}) at a radius of 206 km [this profile has values $v_1 = 29.08$ m s^{-1} and $v_2 = -10.92$ m s^{-1} in Eq. (12)]. Because the new calculation was started at a larger radius (800 vs 500 km), we allowed the boundary layer depth to include a variation proportional to $\sqrt{v_g/v_g(R)}$, where $v_g(R)$ is the value of the gradient wind at the starting radius. As for the weaker vortex in Fig. B1, there is only a weak dependence of the maximum value of v_b as the latitude decreases, but there is a comparatively large effect on the secondary circulation characterized by u_b and w_h.

APPENDIX C

Calculation of CAPE

The values of CAPE given in this article are calculated by lifting hypothetical air parcels from the surface until the level of neutral buoyancy (LNB) of the particular parcel. Pseudoadiabatic ascent is assumed, and the latent heat of fusion in the upper troposphere is not accounted for. Integrals of the buoyancy force, proportional to the difference between the virtual temperature of a lifted parcel and that of its environment at a given height, are evaluated over the height ranges of positive buoyancy and negative buoyancy using a trapezoidal method

with a height interval of 100 m. The sum of the positive and negative integrals for an air parcel lifted from the surface gives the CAPE. The calculations use Bolton's formula (Bolton 1980) to evaluate the pseudoequivalent potential temperature and the formula given in Emanuel (1994, 116, Eq. (4.4.13) to calculate the saturation vapor pressure.

REFERENCES

Bister, M., and K. A. Emanuel, 1998: Dissipative heating and hurricane intensity. *Meteor. Atmos. Phys.,* **65,** 233–240, doi:10.1007/BF01030791.

Black, P. G., and Coauthors, 2007: Air–sea exchange in hurricanes: Synthesis of observations from the coupled boundary layer air–sea transfer experiment. *Bull. Amer. Meteor. Soc.,* **88,** 357–374, doi:10.1175/BAMS-88-3-357.

Bolton, D., 1980: The computation of equivalent potential temperature. *Mon. Wea. Rev.,* **108,** 1046–1053, doi:10.1175/1520-0493(1980)108<1046:TCOEPT>2.0.CO;2.

Braun, S. A., and W.-K. Tao, 2000: Sensitivity of high-resolution simulations of Hurricane Bob (1991) to planetary boundary layer parameterizations. *Mon. Wea. Rev.,* **128,** 3941–3961, doi:10.1175/1520-0493(2000)129<3941:SOHRSO>2.0.CO;2.

Bryan, G. H., and R. Rotunno, 2009: Evaluation of an analytical model for the maximum intensity of tropical cyclones. *J. Atmos. Sci.,* **66,** 3042–3060, doi:10.1175/2009JAS3038.1.

Bui, H. H., R. K. Smith, M. T. Montgomery, and J. Peng, 2009: Balanced and unbalanced aspects of tropical cyclone intensification. *Quart. J. Roy. Meteor. Soc.,* **135,** 1715–1731, doi:10.1002/qj.502.

Carrier, G. F., 1971: The intensification of hurricanes. *J. Fluid Mech.,* **49,** 145–158, doi:10.1017/S0022112071001976.

Craig, G. C., and S. L. Gray, 1996: CISK or WISHE as the mechanism for tropical cyclone intensification. *J. Atmos. Sci.,* **53,** 3528–3540, doi:10.1175/1520-0469(1996)053<3528:COWATM>2.0.CO;2.

DeMaria, M., and J. D. Pickle, 1988: A simplified system of equations for simulation of tropical cyclones. *J. Atmos. Sci.,* **45,** 1542–1554, doi:10.1175/1520-0469(1988)045<1542:ASSOEF>2.0.CO;2.

Eliassen, A., 1951: Slow thermally or frictionally controlled meridional circulation in a circular vortex. *Astrophys. Norv.,* **5,** 19–60.

Emanuel, K. A., 1986: An air–sea interaction theory for tropical cyclones. Part I: Steady-state maintenance. *J. Atmos. Sci.,* **43,** 585–604, doi:10.1175/1520-0469(1986)043<0585:AASITF>2.0.CO;2.

——, 1994: *Atmospheric Convection.* Oxford University Press, 592 pp.

——, 1995: Sensitivity of tropical cyclones to surface exchange coefficients and a revised steady-state model incorporating eye dynamics. *J. Atmos. Sci.,* **52,** 3969–3976, doi:10.1175/1520-0469(1995)052<3969:SOTCTS>2.0.CO;2.

——, 2003: Tropical cyclones. *Annu. Rev. Earth Planet. Sci.,* **31,** 75–104, doi:10.1146/annurev.earth.31.100901.141259.

——, 2012: Self-stratification of tropical cyclone outflow. Part II: Implications for storm intensification. *J. Atmos. Sci.,* **69,** 988–996, doi:10.1175/JAS-D-11-0177.1.

Fang, J., and F. Zhang, 2011: Evolution of multiscale vortices in the development of Hurricane Dolly (2008). *J. Atmos. Sci.,* **68,** 103–122, doi:10.1175/2010JAS3522.1.

Gopalakrishnan, S. G., F. Marks, X. Zhang, J.-W. Bao, K.-S. Yeh, and R. Atlas, 2011: The experimental HWRF system: A study on the influence of horizontal resolution on the structure and intensity changes in tropical cyclones using an idealized framework. *Mon. Wea. Rev.,* **139,** 1762–1784, doi:10.1175/2010MWR3535.1.

Grell, G. A., J. Dudhia, and D. R. Stauffer, 1995: A description of the fifth-generation Penn State/NCAR mesoscale model (MM5). NCAR Tech. Note NCAR/TN-398+STR, 121 pp., doi:10.5065/D60Z716B.

Haynes, P., and M. E. McIntyre, 1987: On the evolution of vorticity and potential vorticity in the presence of diabatic heating and frictional or other forces. *J. Atmos. Sci.,* **44,** 828–841, doi:10.1175/1520-0469(1987)044<0828:OTEOVA>2.0.CO;2.

Holton, J. R., 2004: *An Introduction to Dynamic Meteorology.* 4th ed. Academic Press, 535 pp.

Juckes, M., and R. K. Smith, 2000: Convective destabilization by upper-level troughs. *Quart. J. Roy. Meteor. Soc.,* **126,** 111–123, doi:10.1002/qj.49712656206.

Kaplan, J., and M. DeMaria, 2003: Large-scale characteristics of rapidly intensifying tropical cyclones in the North Atlantic basin. *Wea. Forecasting,* **18,** 1093–1108, doi:10.1175/1520-0434(2003)018<1093:LCORIT>2.0.CO;2.

Kepert, J. D., 2010: Slab- and height-resolving models of the tropical cyclone boundary layer. Part I: Comparing the simulations. *Quart. J. Roy. Meteor. Soc.,* **136,** 1686–1699, doi:10.1002/qj.667.

——, 2012: Choosing a boundary layer parameterization for tropical cyclone modeling. *Mon. Wea. Rev.,* **140,** 1427–1445, doi:10.1175/MWR-D-11-00217.1.

Li, T., X. Ge, M. Peng, and W. Wang, 2012: Dependence of tropical cyclone intensification on the Coriolis parameter. *Trop. Cyclone Res. Rev.,* **1,** 242–253.

Montgomery, M. T., and R. K. Smith, 2014: Paradigms for tropical cyclone intensification. *Aust. Meteor. Oceanogr. J.,* **64,** 37–66.

——, V. S. Nguyen, R. K. Smith, and J. Persing, 2009: Do tropical cyclones intensify by WISHE? *Quart. J. Roy. Meteor. Soc.,* **135,** 1697–1714, doi:10.1002/qj.459.

——, R. K. Smith, and V. S. Nguyen, 2010: Sensitivity of tropical-cyclone models to the surface drag coefficient. *Quart. J. Roy. Meteor. Soc.,* **136,** 1945–1953, doi:10.1002/qj.702.

——, J. A. Zhang, and R. K. Smith, 2014: An analysis of the observed low-level structure of rapidly intensifying and mature Hurricane Earl (2010). *Quart. J. Roy. Meteor. Soc.,* **140,** 2132–2146, doi:10.1002/qj.2283.

——, J. Persing, and R. K. Smith, 2015: Putting to rest WISHE-ful misconceptions for tropical cyclone intensification. *J. Adv. Model. Earth Syst.,* doi:10.1002/2014MS000362, in press.

Nguyen, V. S., R. K. Smith, and M. T. Montgomery, 2008: Tropical-cyclone intensification and predictability in three dimensions. *Quart. J. Roy. Meteor. Soc.,* **134,** 563–582, doi:10.1002/qj.235.

Ooyama, K. V., 1964: A dynamical model for the study of tropical cyclone development. *Geofis. Int.,* **4,** 187–198.

——, 1969: Numerical simulation of the life cycle of tropical cyclones. *J. Atmos. Sci.,* **26,** 3–40, doi:10.1175/1520-0469(1969)026<0003:NSOTLC>2.0.CO;2.

——, 1982: Conceptual evolution of the theory and modeling of the tropical cyclone. *J. Meteor. Soc. Japan,* **60,** 369–380.

Persing, J., M. T. Montgomery, J. McWilliams, and R. K. Smith, 2013: Asymmetric and axisymmetric dynamics of tropical cyclones. *Atmos. Chem. Phys.,* **13,** 12 299–12 341, doi:10.5194/acp-13-12299-2013.

Rappin, E. D., M. C. Morgan, and G. J. Tripoli, 2011: The impact of outflow environment on tropical cyclone intensification and structure. *J. Atmos. Sci.,* **68,** 177–194, doi:10.1175/2009JAS2970.1.

Rotunno, R., 2014: Secondary circulations in rotating-flow boundary layers. *Aust. Meteor. Oceanogr. J.,* **64,** 27–35.

——, and K. A. Emanuel, 1987: An air–sea interaction theory for tropical cyclones. Part II: Evolutionary study using a nonhydrostatic axisymmetric numerical model. *J. Atmos. Sci.,* **44,** 542–561, doi:10.1175/1520-0469(1987)044<0542:AAITFT>2.0.CO;2.

Smith, R. K., 2003: A simple model of the hurricane boundary layer. *Quart. J. Roy. Meteor. Soc.,* **129,** 1007–1027, doi:10.1256/qj.01.197.

——, 2006: Accurate determination of a balanced axisymmetric vortex in a compressible atmosphere. *Tellus,* **58A,** 98–103, doi:10.1111/j.1600-0870.2006.00149.x.

——, and M. T. Montgomery, 2008: Balanced boundary layers used in hurricane models. *Quart. J. Roy. Meteor. Soc.,* **134,** 1385–1395, doi:10.1002/qj.296.

——, and S. Vogl, 2008: A simple model of the hurricane boundary layer revisited. *Quart. J. Roy. Meteor. Soc.,* **134,** 337–351, doi:10.1002/qj.216.

——, and M. T. Montgomery, 2010: Hurricane boundary-layer theory. *Quart. J. Roy. Meteor. Soc.,* **136,** 1665–1670, doi:10.1002/qj.679.

——, and G. L. Thomsen, 2010: Dependence of tropical-cyclone intensification on the boundary-layer representation in a numerical model. *Quart. J. Roy. Meteor. Soc.,* **136,** 1671–1685, doi:10.1002/qj.687.

——, M. T. Montgomery, and V. S. Nguyen, 2009: Tropical cyclone spin-up revisited. *Quart. J. Roy. Meteor. Soc.,* **135,** 1321–1335, doi:10.1002/qj.428.

——, C. W. Schmidt, and M. T. Montgomery, 2011: An investigation of rotational influences on tropical-cyclone size and intensity. *Quart. J. Roy. Meteor. Soc.,* **137,** 1841–1855, doi:10.1002/qj.862.

——, M. T. Montgomery, and J. Persing, 2014: On steady-state tropical cyclones. *Quart. J. Roy. Meteor. Soc.,* **140,** 2638–2649, doi:10.1002/qj.2329.

Turner, J. S., and D. K. Lilly, 1963: The carbonated-water tornado vortex. *J. Atmos. Sci.,* **20,** 468–471, doi:10.1175/1520-0469(1963)020<0468:TCWTV>2.0.CO;2.

Vogl, S., and R. K. Smith, 2009: Limitations of a linear model for the hurricane boundary layer. *Quart. J. Roy. Meteor. Soc.,* **135,** 839–850, doi:10.1002/qj.390.

Willoughby, H. E., 1979: Forced secondary circulations in hurricanes. *J. Geophys. Res.,* **84,** 3173–3183, doi:10.1029/JC084iC06p03173.